Comparative Adhesion of Chemically and Physically Crosslinked Poly(Acrylic Acid)-Based Hydrogels to Soft Tissues

Edward J. Cozens,[1,2] Nima Roohpour[3] and Julien E. Gautrot[1,2]*

[1]Institute of Bioengineering and [2]School of Engineering and Materials Science, Queen Mary, University of London, Mile End Road, London, E1 4NS, UK.

[3]Consumer Healthcare R&D, GlaxoSmithKline, St George's Avenue, Weybridge, Surrey, KT13 ODE, UK.

[*]Corresponding author. j.gautrot@qmul.ac.uk

Abstract

In the design of polymeric biomaterials for soft tissue adhesion, careful regulation of the interactions between the material and soft tissue is critical. In order to improve the efficacy of bioadhesives, a greater understanding of the relationship between their chemical design and resulting adhesion mechanisms is required. In this work, poly(acrylic acid) (PAA) was functionalised either through bromoalkene functionalisation via nucleophilic substitution or via 4-(4,6-dimethoxy-1,3,5-triazin-2-yl)-4-methylmorpholinium chloride (DMTMM)-mediated conjugation. Novel PAA-based hydrogels were developed through different types (chemistry) of crosslinks and crosslinking mechanisms. Two of these gels were crosslinked through UV initiation using Irgacure 2959 as the photoinitiator, another gel used visible light-mediated crosslinking with eosin Y as the photoinitiator, and the final gel utilised physical crosslinking through the interaction between boronic acid moieties and the polysaccharide mannan. Oscillatory rheometry was used to characterise the mechanical properties of the different gels, including their gelation kinetics. Tensile testing was used to characterise the adhesion of the different gels to hydroxyl and methacrylate self-assembled monolayers (SAMs), as a means of studying adhesion to interfaces with defined surface chemistry. Finally, adhesion to soft tissues (porcine epicardium and keratinized gingiva) was studied through lap shear and tensile testing. Our results indicate a variety of factors responsible for hydrogel/soft tissue adhesion; these include the tissue mechanics, bulk mechanics of the gel, weak non-specific adhesion forces, and strong covalent bonding. Tests confirm the effect of tissue biochemistry on adhesion, with thiyl-bonded gels displaying particularly strong adhesion to tissues (particularly the epicardium). It is hoped that the results presented provide insight for the improved rational design of biomaterials for tissue adhesion.

1. Introduction

In the last few decades, a diversity of bioadhesive formulations have been developed and are finding increasing clinical applications to address medical conditions and enable new therapeutic and surgical technologies. Bioadhesives can be applied externally, commonly as topical medications, in applications such as wound closure and autologous skin grafts.[1–3] Additionally, bioadhesives can be used in intracorporal conditions to promote bonding or sealing of tissues and membranes, often in contact with other organs and physiological fluids. These internal applications can include chronic organ repair and bleeding control,[4,5] drug delivery,[6] epicardial placement and stem cell delivery,[7,8] degradable adhesives for tissue regeneration,[9] and mucoadhesives for denture adhesion.[10–12] In contrast with externally-applied bioadhesives, in intracorporal conditions, factors such as the adhesives ability to bond to wet surfaces are critical. Furthermore, in applications such as tissue regeneration, bioadhesives typically require additional complex functionality due to their roles in cell attachment and differentiation.[87] Overall, a critical engineering parameter is the nature of the interactions occurring between the bioadhesive and corresponding soft tissue.

Poly(acrylic acid) (PAA) hydrogels have interesting properties such as stimuli responsive behaviour and high hydrophilicity, due to their high density of carboxyl groups. These groups are readily ionisable, leading to the expansion of the polymer chain conformation, due to increased repulsion between carboxylate groups. Consequently, PAA will reversibly swell/collapse, depending on the pH and ionic strength of the environment.[13,14] This has led to the application of PAA-based materials in microdevices and sensors.[15] Moreover, due to its excellent biocompatability, PAA is commonly applied as mucoadhesives for drug delivery,[12,16–18] as well as surface coatings for biomedical devices.[19,20] Hydrogels can either be classed as chemical gels, where the crosslinks are permanent covalent bonds, or physical gels, where the crosslinks are non-permanent and a result of either physical entanglement of the network or non-covalent bonding such as hydrogen bonds and ionic bonding.[21] In order to form crosslinks within a hydrogel, the polymer backbone can be functionalised with specific reactive moieties. The presence of carboxyl groups in PAA enables direct functionalisation with amines through the well-established EDC/NHS[22,23] and DCC/DMAP[24,25] conjugation methods. Functionalisation of hydrogels enables their chemical crosslinking via a range of approaches, from radical coupling such as thiol-ene chemistry[26,27] and methacrylate polymerisations[28,29], to tyramine mediated ligation[30,31] and disulfide bond formation.[32–34] In addition to such chemical crosslinks, in PAA gels, physical crosslinking inherently contributes to the mechanics of the networks, via secondary hydrogen bonds that crosslink polymer chains. PAA gels will also form physically entangled structures, in which polymer chains are physically trapped, resulting in further non-covalent crosslinks.[35] Hence, a complex set of chemical and physical bonds typically determines the physical properties of PAA hydrogels.

Hydrogels can be chemically crosslinked using a photoinitiator upon exposure to UV or visible light.[31,36–38] This typically requires radical reactive groups on the polymer backbone, such as alkenes and thiols (for thiol-ene coupling).[26,27] Although Irgacure 2959 (I-2959) and Lithium phenyl-2,4,6-trimethylbenzoylphosphinate (LAP)[39] are widely used UV-sensitive photoinitiators, their use for visible light initiation is not possible, due to their near zero extinction coefficient at wavelengths greater than 400 nm.[40] Instead, eosin Y is an attractive option for visible light-mediated photoinitiation, as it is cytocompatible, FDA-approved, highly water soluble and can be excited in the green region of the visible spectrum (450 – 550 nm).[41] In thiol-ene coupling, the excitation of eosin Y by visible light exposure results in hydrogen abstraction from a sulfhydryl group to create a thiyl radical. These thiyl radicals then initiate a rapid and orthogonal thiol-ene gelation reaction (specifically with alkenes).[40,41] In order to further enhance radical generation, the use of eosin Y is often coupled with a co-initiator, leading to faster and more effective functional group conversion.[40,41] For example, Noshadi et al. generated visible light crosslinked gelatin-based hydrogels, using eosin Y as a photoinitiator, triethanolamine (TEA) as a co-initiator, and N-vinylcaprolactam (VC) as a co-monomer. These gels had compressive moduli in the range of 5 – 56 kPa, depending on the concentration of the co-initiator and co-monomer used.[41] However, due to potential cytotoxicity concerns associated with the use of co-initiators such as triethanolamine,[42,43] recent literature has also focussed on using eosin Y alone for radical generation.[31,42,43] Thiol-ene radical coupling is a technique that is increasingly being used in areas such as the biofunctionalisation of biomaterials[26,44] and the formation of 3D hydrogels encapsulating cells.[45–47] The use of thiol-ene chemistry for the design of hydrogels is an attractive technique due to its tolerance to many different reaction conditions and the generally mild conditions required, as well as the simple and clearly defined reaction pathways, and the availability of alkene functions as side chains of macromolecules.[48]

In comparison to chemical hydrogels, hydrogels crosslinked through physical interactions possess an intrinsic responsiveness to environmental stimuli, as these physical crosslinking interactions are reversible. However, physical hydrogels often lack the stability found within covalently crosslinked hydrogels. To combine the advantages of both physical and chemical hydrogels, dynamic covalent crosslinks, such as disulfide bonds, can be used. Disulfide bonds are capable of being broken down or reforming via the physiologically-relevant reduction/oxidation and thiol-disulfide exchange reactions,[49] and they are emerging as promising candidates to enable *in situ* crosslinking of hydrogels.[50,51]

Boronic acid-based materials and interfaces have also generated significant interest in the biomedical field due to their ability to form reversible quasi-covalent bonds with a number of biologically

important molecules bearing diol functionalities, such as glucose and a wide range of polysaccharides.[52] The reversible covalent interaction of boronic acids with diols has proven sufficiently strong that it enables binding of saccharides at mM or sub-mM levels.[53] Due to this ability to bind saccharides at low concentrations, along with the wide range of molecules boronic acids can bind to, boronic acids have been widely exploited in various biosensor applications.[52–54] In addition, as boronate esters are pH sensitive and undergo hydrolysis in acidic conditions, boronic acid-crosslinked polymers have been extensively studied as stimuli-responsive hydrogels.[52,55] For example, Heleg-Shabtai *et al.* demonstrated the use of Gossypol-crosslinked boronic acid-modified hydrogels as a functional matrix for the controlled release of an anticancer drug.[55] Furthermore, due to the reversibility of the covalent bonding between boronic acids and diols, hydrogels crosslinked with boronic acid have demonstrated self-healing properties at neutral and acidic pH.[56]

The crosslinking strategy used to generate a gel has a critical influence on its mechanical properties,[21,57] but also its adhesive performance. Most covalently crosslinked hydrogels display relatively brittle properties with limited stretchability and toughness.[57] However, hydrogels formed through a synergy of physical and covalent crosslinks, have been shown to demonstrate significantly enhanced stretchability and toughness.[57,58] This behaviour can result from the introduction of energy dissipating mechanisms in the form of sacrificial physical bonds. Upon loading of a material, this network of physical bonds ruptures and dissipates energy, leaving the covalent bonding intact.[59,60] Furthermore, these physical bonds show the ability to re-form upon unloading of a sample, leading to the recovery of these energy dissipating mechanisms. As an example, Sun *et al.* synthesised hydrogels from a network of ionic and covalent crosslinks, leading to a gel with high toughness which can be stretched to beyond 20 times its initial length.[57]

In order to evaluate the benefit of different coupling chemistries on hydrogel mechanics and soft tissue adhesion, side-by-side comparison is required. In this work, we synthesised a range of PAA-based hydrogels displaying different crosslinking chemistries and able to bond to surfaces and soft tissues via different mechanisms. The coupling strategies targeted aimed to make use of the biochemistry typically associated with cell membranes and epithelial tissues, to ensure bonding and crosslinking via the same moieties. We investigate the influence of such chemical design on the resulting mechanical and adhesive properties. Four different crosslinking chemistries were studied. Two of these gels were formed through UV irradiation in the presence of Irgacure 2959, to mediate thiol-ene and thiol-thiol couplings, making use of the natural presence of cysteines in membrane bound and extra-cellular matrix proteins. Another strategy explored was the use of tyramine coupling, initiated by visible light in the presence of the photoinitiator eosin Y, enabling simultaneous coupling

to tissues via reaction with tyrosine residues.[61,62] The final strategy developed the use of boronic acid moieties to crosslink the polysaccharide mannan, resulting in more dynamic crosslinks, and contributing to tissue bonding via membrane proteoglycans and glycosaminoglycans. Parallel plate shear rheometry allowed the characterisation of the complex evolution of the rheological and shear mechanical properties of these materials prior, during and after curing. The bonding strength of these PAA hydrogels to two soft epithelial tissues, the gingiva (which structure and homeostasis is regulated by gingival keratinocytes) and the epicardium (a membrane to which adhesion is particularly relevant for epicardial placement strategies[63,64]), was then explored. The systematic study of the impact of chemical design on the mechanical behaviour and bioadhesive properties of PAA gels is proposed to be essential to improve their performance and the rational design of other hydrogel adhesives. Adhesive properties were characterised via tensile and lap shear testing, allowing the correlation of adhesion strength and hydrogel chemistry. To enable better understanding of the adhesion process, adhesion to model surfaces displaying hydroxyl and methacrylate residues was also quantified.

2. Experimental Section

2.1. Chemicals and materials

Poly(acrylic acid) (PAA, average M_V 450 kDa, determined by the supplier), 3-(bromomethyl)phenylboronic acid (90%), 5-bromo-1-pentene (95%), 2-hydroxy-4'-(2-hydroxyethoxy)-2-methylpropiophenone (Irgacure 2959, 98%), toluene (anhydrous, 99.8%), triethylamine (≥99.5%), Dulbecco's phosphate buffered saline (PBS), cystamine dihydrochloride (≥98%), tyramine hydrochloride (≥98%), methanol (MeOH, 99.9%), 3-(trimethoxysilyl)propyl methacrylate (98%), mannan from Saccharomyces cerevisiae (prepared by alkaline extraction), DL-Dithiothreitol (DTT, ≥98%), diethyl ether (99%), deuterium oxide (D2O, 99.9 atom % D), dimethyl sulfoxide-d6 (DMSO-d6, 99.9 atom % D), poly(ethylene glycol) dithiol (PEGDT, average M_n 1 kDa, determined by the supplier) and eosin Y (99%) were purchased from Sigma-Aldrich and used as received. 4-(4,6-dimethoxy-1,3,5-triazin-2-yl)-4-methylmorpholinium chloride (DMTMM, >98%) was purchased from Tokyo Chemical Industry UK Ltd. Dimethylformamide (DMF, ≥99.9%) was purchased from VWR Chemicals. Chloroform-D (CDCl3, 99.8%) was purchased from Cambridge Isotope Laboratories Inc. Cellulose ester dialysis membranes (3.5-5 kDa MWCO) were purchased from Spectrum Laboratories Inc. All Plasma treatment was carried out using a Henniker Plasma Vacuum System HPT-200. pH measurements were taken using a Mettler Toledo, SG2 – SevenGo pH meter.

2.2. Functionalisation of poly(acrylic acid)

Amine ligation via DMTMM-mediated conjugation

The conjugation of PAA with amines was carried out using DMTMM, following a procedure adapted from the literature.[30,31] For functionalisation of PAA (450 kDa) with tyramine, PAA (1.5 g, 20.8 mmol) was initially dissolved in deionized water (30 mL). The pH of the solution was adjusted to 5.5 using 2 M NaOH, following which DMTMM (2.857 g, 10.4 mmol) was added and left to dissolve. Tyramine hydrochloride (1.429 g, 8.26 mmol) was dissolved separately in deionized water (20 mL) and the pH of this solution was adjusted to 5.5 using 50 mM NaOH. This solution was then added dropwise to the polymer solution, which was then left at 37˚C for 24 h. The conditions used equate to molar equivalences of 0.4:0.5:1 for tyramine:DMTMM:PAA. The cooled reaction mixture was then precipitated in acetone three times, re-dissolving the resulting material in deionised water each time, and the polymer was left for several days to dry under reduced pressure. After drying, the polymer was re-dissolved in deionized water (25 mL) and then dialyzed in a solution of 150 mM NaCl for two days, whilst changing the dialysis solution at least 3 times a day. Next, the polymer was dialyzed in deionized water for a further two days, whilst again changing the dialysis solution at least three times a day. Following dialysis, the resulting polymer was frozen in liquid nitrogen and freeze dried for one to two days, until fully dry.

PAA was also functionalised with cystamine via DMTMM conjugation. This was achieved through a two-step procedure involving initial functionalisation with cystamine followed by cleavage of the disulfide bond using dithiothreitol (DTT).[32,33] For functionalisation of PAA (450 kDa) with cystamine, PAA (300 mg, 4.17 mmol) was initially dissolved in deionized water (6 mL). The pH of the solution was adjusted to 5.5 using 5 M NaOH, following which DMTMM (572 mg, 2.07 mmol) was added and left to dissolve. Cystamine dihydrochloride (466 mg, 2.07 mmol) was dissolved separately in deionized water (4 mL) and the pH of the resulting solution was adjusted to 5.5 using 50 mM NaOH. This solution was then added dropwise to the polymer solution and left at 37˚C overnight. After reacting overnight, the pH of the polymer solution was changed to 9.0 using a solution of 5 M NaOH. DTT (424 mg, 2.75 mmol) was dissolved separately in deionized water (5 mL) and the pH of this solution was adjusted to 9.0, using a solution of 500 mM NaOH. This DTT solution was then added dropwise to the polymer solution, which was then left overnight at room temperature. These conditions equate to molar equivalences of 0.5:0.5:1 for cystamine:DMTMM:PAA. Next, the reaction mixture was precipitated in acetone three times, from deionized water, and the polymer was then dried under reduced pressure.

Bromoalkene functionalisation via nucleophilic substitution

The procedure for the functionalisation of PAA via conjugation with bromine moieties was adapted from protocols in the literature that investigated the functionalisation of carboxymethylcellulose (CMC)[65] and poly(dimethylaminoethyl methacrylate) (PDMAEMA).[27] For functionalisation of PAA (450 kDa) with bromo pentene, NaOH (104 mg, 2.6 mmol) was initially dissolved in deionized water (2.63 mL). PAA (250 mg, 3.47 mmol) was then added, followed by heating of the solution to 70˚C. 5-bromo-1-pentene (130 mg, 872 µmol) was dissolved in DMF (0.5 mL) separately and this solution was added dropwise to the polymer solution and then left overnight at 70˚C. These conditions equate to molar equivalences of 0.75:0.25:1 for base:conjugate:PAA. The cooled reaction mixture was precipitated in acetone:diethyl ether (3:1), re-dissolved in deionized water and then precipitated in acetone twice, from deionized water. The polymer was then left for several days to dry under reduced pressure.

For functionalisation of PAA (450 kDa) with boronic acid moieties, PAA (3 g, 41.7 mmol) was initially dissolved in a solution of NaOH (1.25 g, 31.25 mmol) and deionised water (31.54 mL), which was then heated to 70˚C. 3-(bromomethyl)phenylboronic acid (2.241 g, 10.43 mmol) was separately dissolved in DMF (6 mL) and then added to the polymer solution dropwise. These conditions equate to molar equivalences of 0.75:0.25:1 for base:conjugate:PAA. The mixture was left at 70˚C overnight. The cooled reaction mixture was precipitated in acetone:diethyl ether (3:1), re-dissolved in deionized water and then precipitated in acetone twice, from deionized water. The polymer was then left for several days to dry under reduced pressure.

Characterisation of polymers

Fourier Transform Infrared–Attenuated Total Reflectance Spectroscopy (ATR-FTIR) was carried out on polymer samples which had been fully dried and crushed into a powder. Spectra were acquired using a Bruker Tensor 27 with an MCT detector (liquid N_2 cooled), at a resolution of 4 cm^{-1} with a total of 256 scans per run. Nitrogen was run through the system during measurements in order to limit the effects of environmental fluctuations. ^{1}H NMR was used to quantify polymer functionalisation levels. Spectra were obtained using Bruker's 400 MHz spectrometers (Bruker AV 400 and AVIII 400) and data was analysed using Bruker's IconNMR software. Multiple batches were synthesised for each polymer and the corresponding mean values and standard error in functionalisation level are reported.

2.3. Crosslinking of polymers

The protocol for the preparation of gels based on tyramine functionalised PAA was adapted from a previous study that investigated the photo-crosslinking of hyaluronan.[31] Initially, the functionalised PAA was dissolved in PBS. Following this, an eosin Y solution was prepared (50 mg/mL PBS) and added at 0.15% molar equivalence relative to the polymer (tyramine residues), based on previous studies.[31]

Visible light curing was applied at an intensity of 40 mW/cm^2 for 5 min. Visible light of controllable intensity was achieved via an OSL2 fiber illuminator from Thorlabs (λ 400-1300 nm). Throughout this article, gels formed through this approach will be referred to as PAA-Tyr hydrogels. For all of the gels generated in this article, solutions were prepared freshly before tests and the photoinitiator, or crosslinking agent, was added the evening before testing to allow for a more homogeneous mixing without the introduction of bubbles.

For gels prepared from cystamine functionalised PAA, the polymers were dissolved in PBS, followed by the addition of 30% molar ratio of Irgacure 2959 relative to the thiol content, which was added in solution form (250 mg/mL MeOH). The photoinitiator concentration used was selected based on previous reports.[66] Gels were cured under UV light at an intensity of 17 mW/cm^2 for 10 min. The UV light source used was an Omnicure series 1500 mercury lamp (λ 280-600 nm). An ILT 1400-A radiometer photometer from International Light Technologies Inc. was used to measure UV light intensities. Throughout the article, these gels are referred to as PAA-Cys hydrogels.

Mannan was used to physically crosslink boronic acid-functionalised PAA. Mannan was dissolved in PBS (250 mg/mL), before addition to the polymer solutions. For preparation of the gels, the polymer was initially dissolved in PBS, and then once fully dissolved the mannan solution was added at a level of 10% molar equivalence relative to boronic acid (saccharide vs. boronic acid moieties). Due to the high density of hydroxyl groups available per mannan molecule, this relatively low concentrations was sufficient. Throughout the article, these gels are referred to by the notation PAA-BA hydrogels.

For preparation of gels based on 5-bromo-1-pentene-functionalised PAA, the polymer was initially dissolved in PBS. PEGDT (225 mg/mL PBS) and Irgacure 2959 solutions (250 mg/mL MeOH) were prepared, and PEGDT was then added at a molar ratio of alkene:thiol of 2:1, followed by the addition of Irgacure 2959 at a molar ratio of 5% relative to the alkene level. Both these concentrations were selected based on previously published results.[47] UV initiation was carried out at an intensity of 17 mW/cm^2 for 2 min, using the UV source detailed earlier. Throughout this article, these gels are referred to by the notation PAA-BP hydrogels.

We note that none of the hydrogels developed were incubated or washed, prior to characterisation, to allow better comparison of the different mechanical/rheological characterisation data and to avoid dissolution and weakening of physically crosslinked hydrogels. We also highlight that all concentrations of PAA polymer backbones used are expressed as w/v%, with respect to the corresponding functionalised polymer backbone, without taking into account additional crosslinkers (e.g. mannan).

2.4. Hydrogel characterisation via oscillatory rheometry

The mechanical properties of gels were characterised by oscillatory rheology, using a TA Discovery HR-3 hybrid rheometer with a 20 mm diameter standard Peltier plate geometry installed. Gels were characterised using time sweeps, frequency sweeps, amplitude (strain) sweeps and through stress relaxation profiles. Time sweeps were used to monitor the change in mechanics before, during and after curing of the gels; for these tests, oscillating frequencies of 1 Hz and oscillating displacements of 10^{-4} rad (0.2% strain) were used. The frequency sweeps were performed from 0.1-100 Hz at an oscillating displacement of 10^{-4} rad (0.2% strain). Amplitude sweeps were performed at an oscillating frequency of 1 Hz. For stress relaxation experiments, gels were subjected to a 2% strain (2 s strain rise time) and the subsequent drop in stress was monitored.

In order to achieve sufficient bonding between the hydrogels and the upper and lower geometries of the rheometer, functionalised glass coverslips were used.[65] These coverslips were produced industrially with high geometrical accuracy and were cleaned prior to functionalisation. They were glued in place using Loctite super glue and could subsequently be readily removed by immersion in acetone. For functionalisation, glass coverslips (20 mm diameter) were plasma oxidized (10 min, air) and then placed in a solution of anhydrous toluene (30 mL), 3-(trimethoxysilyl)propyl methacrylate (30 µL) and triethylamine (50 µL), and left overnight. They were then washed with deionised water, followed by ethanol, and then dried under a stream of nitrogen.

Curing of the gels was via photo-irradiation through the lower surface of the gels using a TA Instruments UV curing accessory. UV and visible light sources, as detailed in section 2.3, could be applied using this light guide accessory. Prior to starting each experiment light intensities were measured *in situ* through the glass slides. All rheology experiments were repeated at least 3 times and representative curves are shown in all cases. A one-way ANOVA test with Tukey's post hoc analysis was used to determine statistical significance. In all figures, standard errors are reported.

2.5. Preparation of soft tissues

Soft tissue samples were sourced and dissected as described in our previous work.[67] Briefly, epicardial and gingival samples were obtained from freshly obtained porcine tissues (6 to 7-month-old pigs). These were cut into 15 mm^2 samples for testing, with a thickness of approximately 2 mm. In order to accurately account for variations in sample sizes, images were captured for each sample and the area was calculated using ImageJ. All testing was carried out within 48 hours from the day fresh samples were obtained and samples were stored in PBS in the fridge prior to tests. Gingival samples were extracted using a scalpel from the lingual side of the lower mandible. These samples were taken from the region of the keratinized attached gingiva which is the gingival portion that lies between the free

gingival groove and the mucogingival junction. Epicardial samples were extracted from the wall of the left and right ventricles. These samples were taken from the healthy areas of the myocardium away from any major adipose tissue deposits or prominent blood vessels. For each adhesion experiment, results were obtained from samples extracted from a minimum of two separate animals.

2.6. Characterisation of hydrogel bonding

Tensile bond adhesion testing

Tensile bond tests were carried out using a TA Discovery HR-3 hybrid rheometer in axial mode, moving at a constant linear rate of 2.5 mm/min and with an angular velocity of 0 rad/s. Testing utilised a 20 mm Peltier plate geometry and samples were loaded in-between the upper and lower plates (similarly to oscillatory rheometry experiments) ensuring there was full gap coverage. Tests were ended when any material bridging the gap between the upper and lower Peltier plates had completely detached or failed. To keep material loading constant between tests and conditions, a gap size of 300 µm was used across experiments. Adhesion tests to self-assembled monolayers (SAMs) were carried out using either plasma treated (10 min, air) or methacrylate functionalised (see section 2.4) glass slides glued to the lower and upper plates. Adhesion tests to soft tissues were carried out using the same 20 mm Peltier plate geometry with a plasma treated (10 min, air) 20 mm glass slide glued to the lower plate. Supplementary Figure 1A shows a diagram of the experimental setup used for the testing of these tissue samples, in which the samples were glued to the upper plate using Loctite Super Glue. To enhance bonding of the tissue samples to the Peltier plate geometry a thin plastic sheet (the lid of a polystyrene plastic petri dish) was placed between the tissue sample and upper plate surface. Adhesion of the gels to glass slides was studied across adhesion tests as this allowed the testing of gel adhesion following *in situ* photo-curing, consistently throughout this study. Similarly to the oscillatory rheometry experiments, *in situ* photo-curing was carried out using the light guide accessory. Sample curing was completed shortly before tensile bond testing was carried out, to minimise the effects of sample drying.

Lap shear adhesion testing

Lap shear experiments for soft tissue testing were performed using an Instron 5967 universal testing system with a 100 N static load cell and lap shear rig installed. Supplementary Figure 1B shows a diagram of the experimental setup used. During testing, a constant extension speed of 10 mm/min was used. For loading of samples, tissue segments were initially glued to a PMMA slide that had been positioned flat on the bench. Approximately 150 µl of polymer solution was pipetted over the tissue surface. A plasma treated (10 min, air) glass slide was then placed on top of the polymer solution/tissue with the hydroxyl-functionalised surface facing downwards. This setup allowed for the

curing of gels with UV light (through the upper surface of the glass slide) before they were loaded into the Instron testing rig. Immediately after UV curing of gels, samples were very carefully loaded into the testing rig ready for tests. Testing was ended when there was no longer any contact between the upper and lower slides.

In the tensile bond and lap shear tests, different failure mechanisms were observed for the gels and these were assessed by a visual inspection of the surfaces following testing. In circumstances where complete debonding of the gel was observed from the glass or tissue substrate, this was characterised as adhesive failure. On the other hand, where the gel remained on both the upper and lower substrates, this was classed as cohesive failure. From the data obtained for the tensile bond and lap shear tests, two parameters were characterised: adhesion strength and energy density. Both were calculated using a custom-built Matlab script. Adhesion strength is defined as the maximum force divided by the initial contact area between the gel and substrate. Energy density is defined as the detachment work (the area under the force-extension curve) divided by the initial contact area between the gel and substrate. In all adhesion tests, experiments were repeated at least 3 times and representative curves are shown in all cases. A one-way ANOVA test with Tukey's post hoc analysis was used to determine statistical significance. In all figures, standard errors are reported.

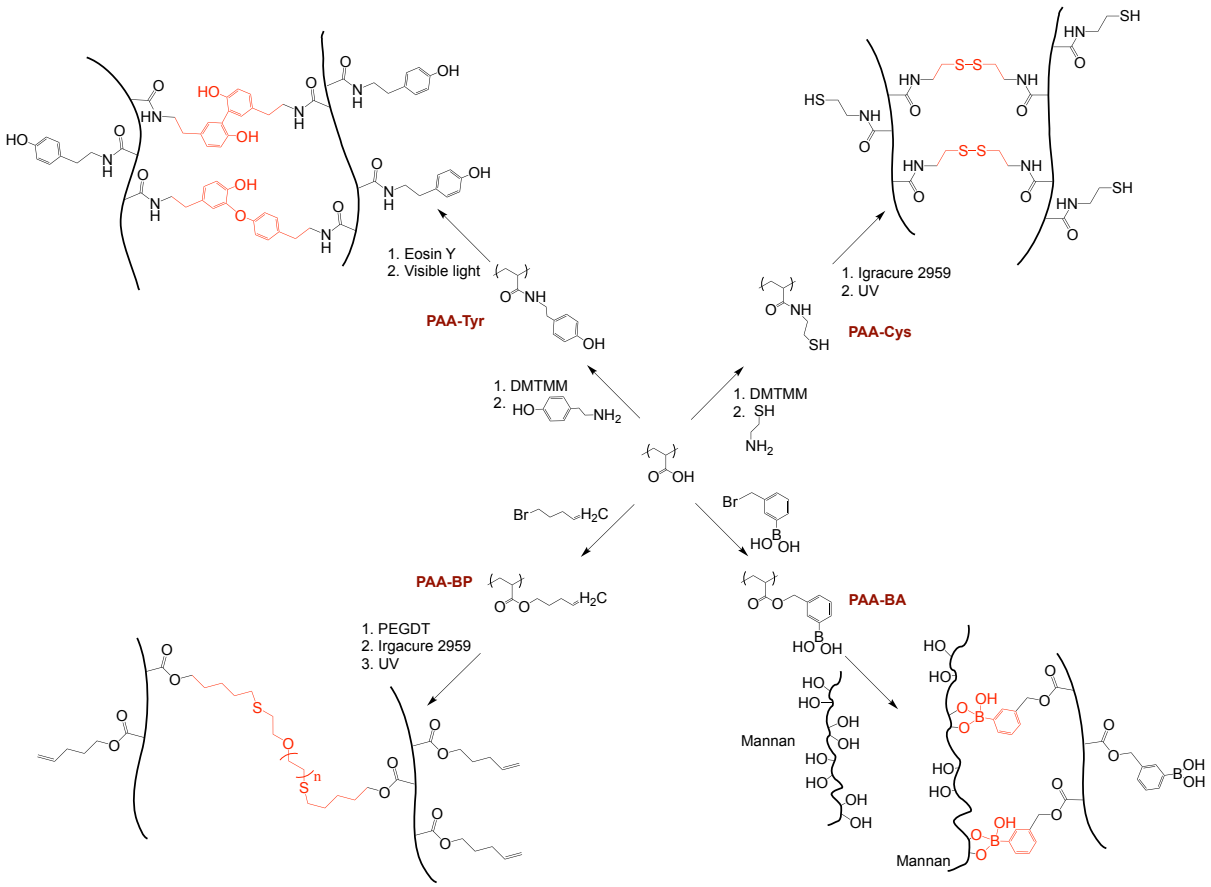

Figure 1. Schematic representation of the process used to form gels based on poly(acrylic acid), functionalised via DMTMM-mediated amine conjugation, or by bromoalkene functionalisation via nucleophilic substitution. PAA-Tyr gels are formed through crosslinking of tyramine molecules under visible light-mediated initiation. PAA-Cys gels are formed from cysteamine-functionalised PAA under UV-mediated initiation. PAA-BP gels are formed through thiol-ene reactions in the presence of UV light, with poly(ethylene glycol) dithiol (PEGDT) as the thiol crosslinker. PAA-BA gels are physically crosslinked through the interaction between boronic acid and the polysaccharide, mannan.

3. Results and Discussion

3.1. Functionalisation of poly(acrylic acid)

To promote the coupling of amines to PAA, we used 4-(4,6-dimethoxy-1,3,5-triazin-2-yl)-4-methylmorpholinium chloride (DMTMM) mediated coupling. Recent reports proposed DMTMM as an alternative to EDC/NHS coupling for ligation of amines and applied it in particular to the functionalisation of Hyaluronan.[30,31,68] This method proceeds through aromatic substitution of the carboxyl group, forming an intermediate that is reactive towards nucleophiles, such as amines.[68,69] Previous studies by Thompson *et al.*[69] and Pelet *et al.*[70] also indicated the efficacy of this method for

the derivatization of PAA. Systematic comparison between the use of DMTMM and EDC/NHS suggests that the former is overall more efficient, not requiring as accurate control over the pH to remain effective,[68] and that DMTMM is stable and soluble in water for significantly greater periods of time.[71,72] As a result, DMTMM-mediated ligation is a promising tool for the functionalisation of polymer derivatives for biomedical and pharmaceutical applications. Hence, DMTMM coupling was selected for the coupling of reactive amines onto PAA. In addition, to tether pentene and toluene boronic acid residues to PAA chains, starting from bromo-carbons, we explored the use of nucleophilic substitution (Figure 1).

PAA was initially functionalised with 5-bromo-1-pentene via nucleophilic substitution. ^{1}H NMR confirmed the structure of the polymer obtained (Supplementary Figure 2), with clear alkene protons observed at 5.0 and 5.8 ppm corresponding to three protons, and a broad peak at 4.0 ppm corresponding to the two protons adjacent to the ester moiety. Overall, a functionalisation level of 4.4 ± 0.4% was achieved and the polymer displayed excellent solubility in aqueous media. Considering the molar mass of the PAA used (450 kDa), this corresponds to 325 alkene residues per chains. FTIR spectra were consistent with this structure (Supplementary Figure 3). A broad O-H stretching band can be observed between 2400 and 3700 cm^{-1}. C-H and C-O stretching bands can be seen at 2970 and 1260 cm^{-1}, respectively. Two O-H bending bands can be observed at 800 and 1440 cm^{-1}, and a strong C=O stretching is observed at 1700 cm^{-1}.[73,74] The presence of alkenes is also confirmed via the =C-H bending band observed at approximately 950 cm^{-1}. In contrast to the FTIR spectra obtained for other functionalised PAA materials in this study, the C=O stretching band is split, forming separate peaks at 1657 and 1710 cm^{-1}. This additional peak at 1657 cm^{-1} corresponds to the significant neutralisation of acids and the formation of sodium acrylate residues.[75]

^{1}H NMR characterisation of boronic acid functionalised PAA, also obtained via nucleophilic substitution, revealed a higher functionalisation level of 17.8 ± 0.3% (Supplementary Figure 4), calculated using the ratio of aromatic peaks to backbone protons. For 5-bromo-1-pentene functionalised PAA, higher pentene functionalisation led to either insolubility of the polymer or slight crosslinking in air. In contrast, the high degree of functionalisation obtained with boronic acid may be attributed to the hydrophilicity of the boronic acid residues, enabling enhanced solubility of the polymer in water. FTIR spectra (Figure S5) confirmed the presence of phenyl boronic acid residues, via the occurrence of B-O stretching vibrations and BO_2 out-of-plane deformations, at 1330 and 700 cm^{-1}, respectively.[76]

Next, tyramine functionalisation via DMTMM-mediated conjugation was investigated. DMTMM was selected as the route for functionalisation of PAA due to the fact that tyramine is highly unstable at

the pH range required for EDC/NHS ligation.[30] ^{1}H NMR spectra indicated an overall lower functionalisation level of 1.8 ± 0.2%, calculated using the ratio of aromatic peaks (protons c-f; Supplementary Figure 6) to backbone protons. FTIR spectra confirmed the presence of additional amide I and II bands (between 1500 and 1700 cm^{-1}), and the coupling of amines to the PAA structure (Supplementary Figure 7).[77,78]

Finally, cysteamine functionalisation (after disulfide cleavage) was confirmed by ^{1}H NMR, with a calculated functionalisation level of 4.5 ± 0.1%, based on the quantification of the integration of the peak corresponding to the protons adjacent to the amide, compared to backbone protons (Supplementary Figure 8). FTIR spectra confirmed such functionalisation, with the occurrence of additional amide bands (between 1500 and 1700 cm^{-1}, see Supplementary Figure 9). However, the S-H bond cannot be identified in corresponding spectra, presumably due to the comparative weakness of this band in FTIR.[78] For all PAA functionalisations explored in this study, the aim was to maximise the degree of functionalisation whilst still maintaining good solubility of the polymers in aqueous solutions. Accordingly, the functionalisation levels achieved for these different polymers corresponded to the highest degree of substitution that we were able to achieve or that was possible without precipitation of the polymer at neutral pH.

3.2. Formation of poly(acrylic acid)-based hydrogels

The rheological properties of the four PAA-based gels were investigated next (Figure 2). Compositions of these hydrogels, and a summary of the conditions used, are presented in

Table **1**. The storage moduli of the gels, taken from the frequency sweeps at 1 Hz (0.2% strain), are reported in Figure 2A. As the gel mechanics are significantly influenced by the polymer concentration, the concentration of functionalised PAA was kept at 15% (w/v). Supplementary Figure 10 shows the evolution of the storage moduli during the curing process for the visible and UV-light photoinitiated gels, where, as an exception, testing was performed with gels at a concentration of 10% (w/v).

PAA-Tyr hydrogels demonstrated gradual stiffening over extended time periods under the action of visible light. Storage moduli reached 40 Pa after 5 min of curing (Supplementary Figure 10), with the value continuing to rise. These relatively weak mechanical properties, together with their slight frequency dependence and stress relaxation profile (Figure 2B-D), indicate covalent crosslinking of these hydrogels. Stress relaxation profiles indicated some energy dissipation, but through a relatively slow process and with some elastic component. This is in agreement with the formation of a low density of covalent crosslinks in this system, possibly as a result of the low functionalisation level achieved for PAA-Tyr, in combination with the slow curing and potentially low reaction efficiency of the system.

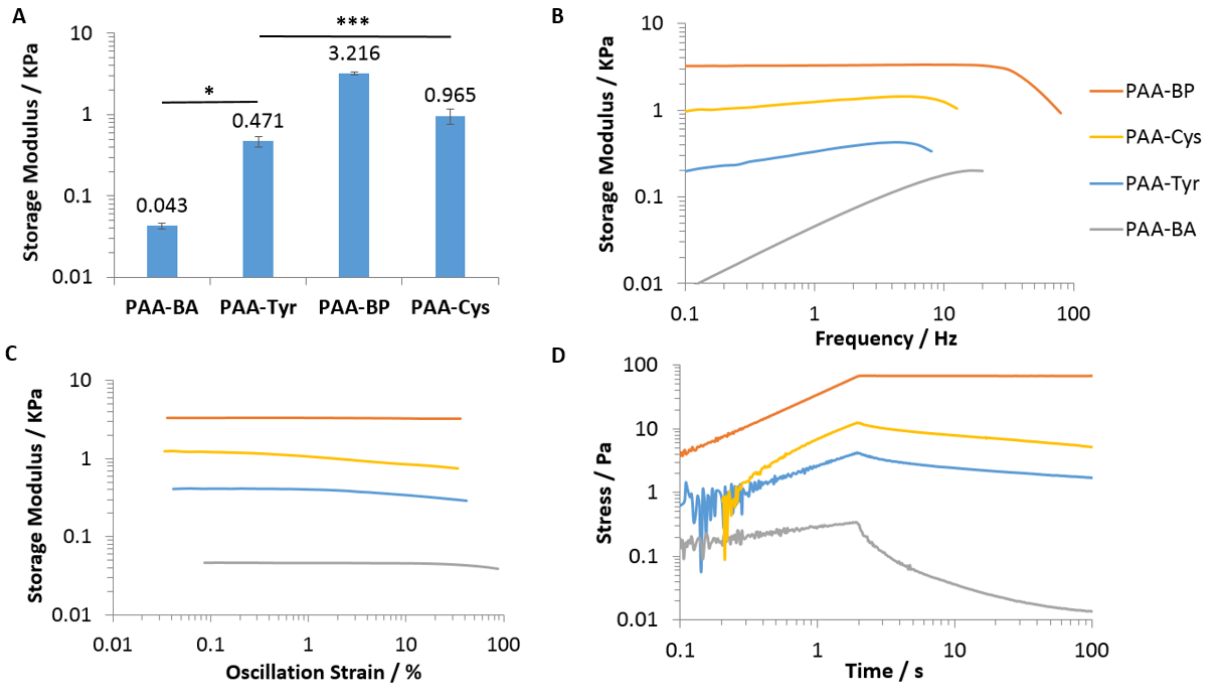

Figure 2. Characterisation of the shear mechanical properties, by oscillatory rheometry, of PAA-based gels under the conditions and concentrations used in adhesion tests (see

Table **1**). Gels are all at a concentration of 15% (w/v) of functionalised PAA in PBS. (A) Storage modulus values of gels. Values taken from frequency sweeps at 1 Hz (0.2% strain). Error bars show standard errors for repeats across samples (sample size $n \geq 3$). *, $p \leq 0.05$. ***, $p \leq 0.001$. (B) Frequency sweeps (0.2% strain) of gels. (C) Strain sweeps (frequency of 1 Hz). (D) Stress relaxation of gels subjected to a rise in strain of 2% over the initial 2 s.

The relatively weak crosslinking achieved for PAA-Tyr gels may also result from the slower generation of radicals compared to other UV-triggered photoinitiators, such as I-2959.[40,41] Indeed, in the presence of I-2959 and the crosslinker poly(ethlyene glycol) dithiol (PEGDT), PAA-BP gels rapidly crosslinked and stiffened upon UV photoirradiation (Supplementary Figure 10), with moduli reaching 3.2 kPa (Figure 2A). Together with the lack of frequency dependence and the low level of stress relaxation observed, this points to a higher density of crosslinks in this system. PAA-Cys hydrogels displayed intermediate moduli, near 970 Pa, with modest levels of frequency dependence and stress relaxation. This is consistent with moduli achieved in comparable gels based on hyaluronic acid, whether mediated by photo-radical oxydation[66] or base-catalysed oxidation.[32,33] However, it was observed that, although PAA-Cys was soluble and generated free flowing viscous solutions prior to curing, the modulus measured was already relatively high. Even though the gels were at neutral pH, this may be a result of some air oxidation (particularly at the edge of the sample and geometries where rheology is most sensitive), leading to the formation of partially crosslinked networks.

In contrast, the physically crosslinked PAA-BA gels displayed the weakest mechanical properties (Figure 2). Despite the high functionalisation level in boronic acid residues, the physical crosslinks, mediated by interactions between boronic acid moieties and mannan chains, resulted in low concentration levels and densities of effective crosslinks. In addition, the striking frequency dependence and high level of stress relaxation of PAA-BA gels was consistent with such physical crosslinks, which are able to dissociate and reform, depending on timescales, in order to dissipate energy and relax chains.[21] Indeed, PAA-BA gels displayed significantly higher stiffnesses at high frequencies compared with low frequencies (gels displayed a storage modulus of 46 Pa at 1 Hz, compared with 176 Pa at 10 Hz; Figure 2B), in agreement with the creation of transient networks that can restructure dynamically after mechanical disruption.[52] Such features are notably utilised to design hydrogels with self-healing properties.[79,80] In comparison, when mannan was added to PAA (unfunctionalised), no significant increase in modulus or change in rheological properties was recorded, indicating that polymer crosslinking is primarily occurring as a result of interactions between boronic acid moieties and mannan (Figure 3). PAA and PAA-BA solutions displayed no measurable stress when sheared in stress relaxation experiments, and physical crosslinks resulting from hydrogen bonding between chains, were too weak and short-lived to results in elastic behaviour (Figure 3D).

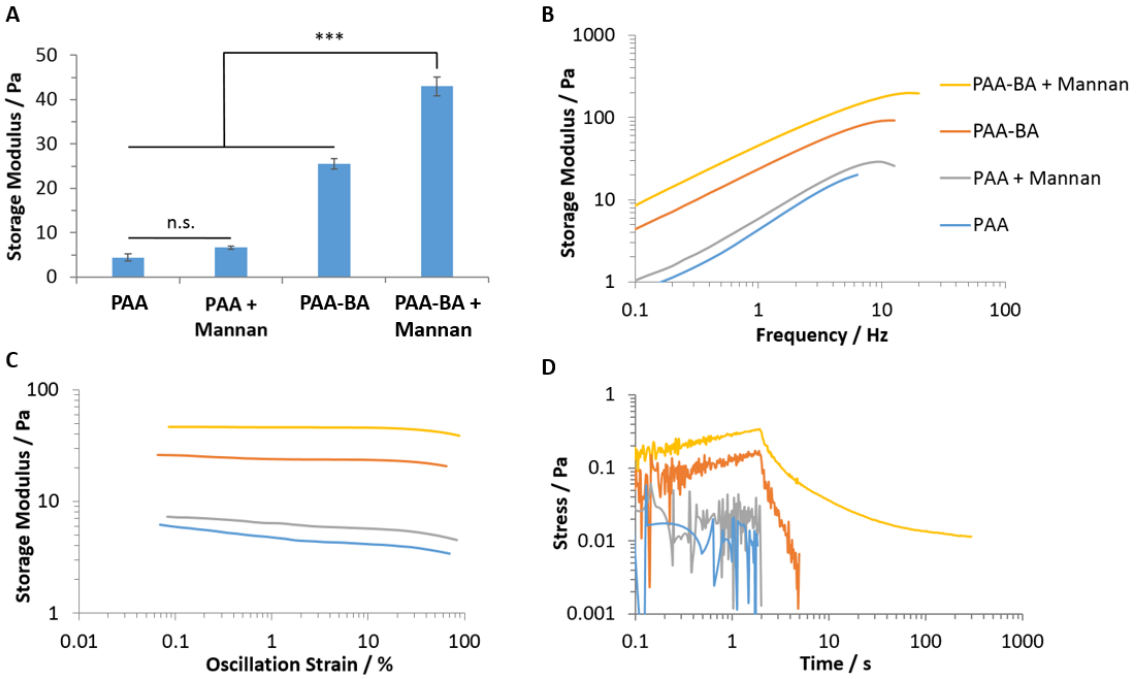

Figure 3. Oscillatory rheometry data for PAA, PAA with mannan, and PAA functionalised with boronic acid (PAA-BA), with and without the addition of mannan. Samples are all at a concentration of 15% (w/v) of PAA (or functionalised PAA) in PBS. Boronic acid functionalisation levels are at 17.8 ± 0.3% and mannan is added at 10% molar equivalence (relative to boronic acid). (A) Storage modulus values of different samples. Values taken from frequency sweeps at 1 Hz (0.2% strain). Error bars show standard errors for repeats across samples (sample size n ≥ 3). ***, p ≤ 0.001. n.s., non-significant. (B) Frequency sweep (0.2% strain) of samples. (C) Corresponding strain sweeps (frequency of 1 Hz). (D) Stress relaxation of corresponding samples subjected to a rise in strain of 2% over the initial 2 s.

In comparison to commonly used tissue adhesives, such as fibrin glues, all of our gels demonstrated good mechanical properties. As an example, the weakest of our gels, PAA-BA, had a storage moduli of 43 Pa (Figure 2A), which is in a similar range to what is often observed for fibrin glues (although this depends on composition), used for stem cell delivery (20 and 80 Pa for concentrations of fibrinogen of 2.5 mg/mL and 5 mg/mL, respectively[8]). The remaining 3 gels we presented had significantly stronger mechanical propertie, with storage moduli in a similar range to recently reported thiol-ene crosslinked poly(2-alkyl-2-oxazoline) hydrogels for epicardial placement and stem cell delivery[8].

3.3. Adhesion of hydrogels to glass and methacrylate monolayers

Prior to characterising adhesion to tissues, we examined the adhesion of the four hydrogels to glass and methacrylate monolayers, which displayed well defined chemistry. This was to examine the contribution of such adhesion to the more complex adhesion profiles measured with tissues. Figure 4 presents the quantification of adhesions between the four different PAA hydrogels tested (

Table **1**) and unfunctionalised glass or methacrylated coverslips, measured via tensile bond testing. A representative force-extension curve is also shown for each gel (Figure 4C). Clearly, radical mediated crosslinking via thiol-ene and thiol-thiol coupling resulted in stronger adhesion to these model substrates. In particular, PAA-BP displayed adhesion strength in the range of 56-89 kPa, and PAA-Cys in the range of 8-17 kPa, in agreement with the ability of these gels to form covalent bonds with methacrylate residues and silanoyl radicals of the associated surfaces. In contrast, PAA-BA and PAA-Tyr were unable to form bonds, whether physical or covalent, with the model substrates studied. It should be noted that the apparent small differences in starting loads between gels resulted from the initial zeroing of loads and the contraction of gels during in situ curing. This trend is also observed in later tensile bond tests performed on soft tissues (Figure 5B and Figure 6B).

Table 1. Summary of the conditions used for the formation of the gels used in the adhesion studies. For all tests, the functionalised PAA polymer is dissolved in PBS and has a M_W of 450 kDa. Polymers used are functionalised with either Tyramine (Tyr), Cysteamine (Cys), 5-bromo-1-pentene (BP) or boronic acid (BA). Functionalisation levels were quantified via NMR.

Polymer	Functionalisation Level (%)[a]	Functionalised PAA Concentration (% (w/v))	Crosslinker Concentration	Photoinitiator Concentration	Crosslinking Mechanism
PAA-Tyr	1.8 ± 0.2	15	N/A	eosin Y (7.5% equiv. to tyramine)	5 min visible light (40 mW/cm^2)
PAA-Cys	4.5 ± 0.1	15	N/A	Irgacure 2959 (30% equiv. to thiol)	10 min UV light (17 mW/cm^2)
PAA-BP	4.4 ± 0.4	15	PEGDT (50% equiv. to alkene)	Irgacure 2959 (5% equiv. to alkene)	2 min UV light (17 mW/cm^2)
PAA-BA	17.8 ± 0.3	15	Mannan (10% equiv. to boronic acid)	N/A	Physical

[a] from ^{1}H NMR.

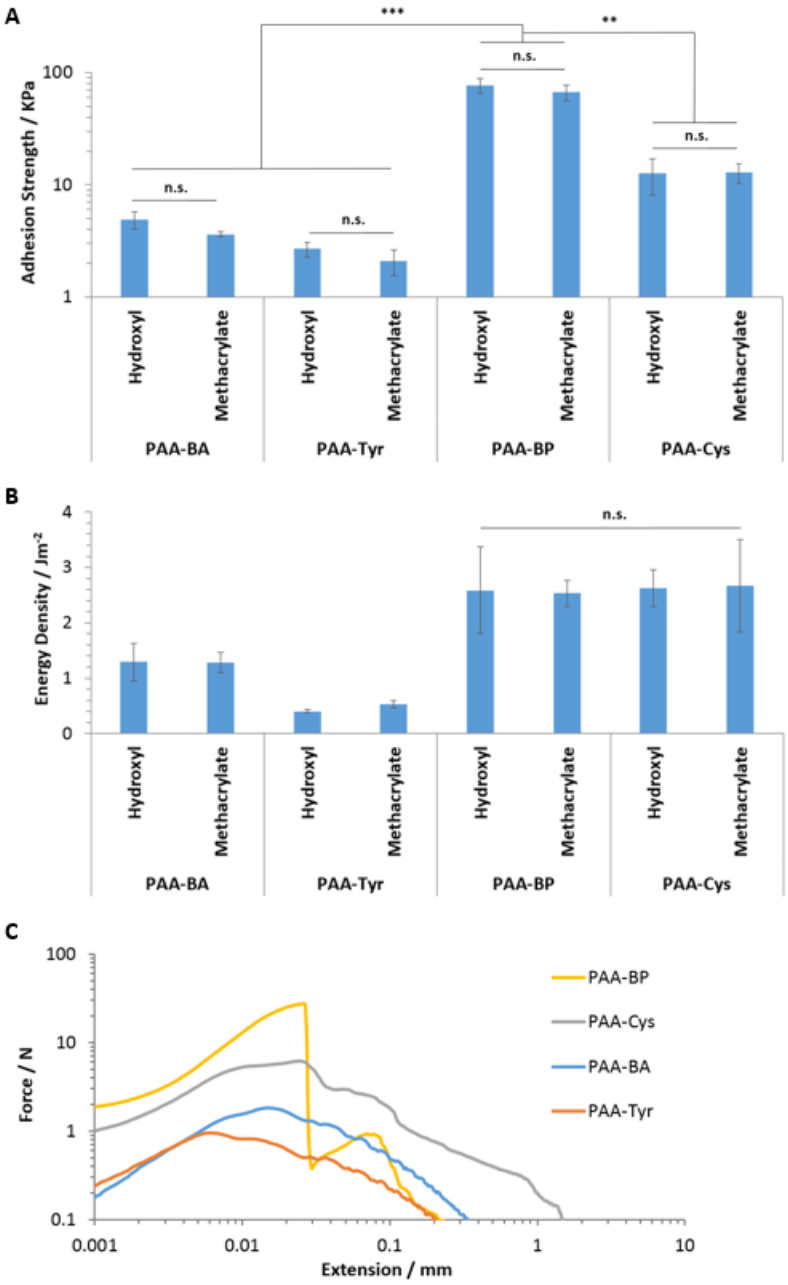

Figure 4. Tensile bond tests for adhesion of PAA-based hydrogels to unfunctionalised and methacrylate glass substrates. (A) Adhesion strength of gels (maximum tensile force (N)/contact area (m^2)). (B) Energy density for gels (detachment work (J)/contact area (m^2)). (C) Force-extension for gels at a constant extension speed of 2.5 mm/min. Error bars show standard errors for repeats across samples (sample size n ≥ 3). **, p ≤ 0.01. ***, p ≤ 0.001. n.s., non-significant.

PAA-BP hydrogels failed adhesively at the glass interface. On the other hand, the other gels tested all displayed relatively elastic properties, with failure associated with a gradual decrease in load (Figure 4C). Accordingly, the adhesion strength of PAA-Cys to SAMs was significantly lower than that of PAA-BP (adhesion strength of PAA-Cys was < 13 KPa; Figure 4A), however the energy densities measured

for both gels were comparable. Given that these two gels have significantly different rheological properties (Figure 2), this similarity in energy density indicates the toughness of PAA-Cys hydrogels. Indeed, PAA-Cys gels failed cohesively, with long fibres bridging the upper and lower substrates, resulting in high energy densities. Most covalently crosslinked hydrogels display relatively brittle properties with limited stretchability and toughness,[57] as observed for PAA-BP gels. The high toughness of PAA-Cys gels is proposed to result from the formation of covalent crosslinks at low density, but with relatively high homogeneity. In particular, no crosslinking molecule is required for such process, whereas PAA-BP relied on crosslinking with PEGDT. In addition, disulfide bonds might remodel under load and reform, acting as energy dissipating elements that may toughen these hydrogels.

Both PAA-BA and PAA-Tyr gels failed cohesively during testing. Interestingly, although PAA-Tyr gels had a storage modulus over an order of magnitude greater than that of PAA-BA gels (Figure 2A), the adhesive properties of PAA-BA gels to the defined surfaces studied, are comparable to those of PAA-Tyr (energy density > 1.28 Jm^{-2} compared with an energy density < 0.53 Jm^{-2} for PAA-Tyr gels; Figure 4B). This may be a result of the higher functionalisation levels for PAA-BA gels coupled with stronger interactions of these gels with the underlying substrates. PAA-BA gels displayed increased adhesion with substrates presenting hydroxyl residues, compared with those presenting methacrylates (4.87 KPa and 3.62 KPa, respectively; Figure 4A), suggesting that the occurrence of hydrogen bonding significantly contributes to adhesion for these gels.

3.4. Characterisation of PAA hydrogel adhesion to soft tissues

The adhesion of PAA hydrogels to gingiva and epicardium was tested next, considering the potential application of these materials for bioadhesives at such interfaces. The adhesion of PAA hydrogels to these tissues (using porcine samples) was carried out via lap shear and tensile bond testing. The experimental setup used for these tests is presented in Supplementary Figure 1. Adhesion was investigated with a functionalised glass slide on the lower surface, to allow photo-curing, and the tissue sample on the upper plate. This setup allowed for curing of some of the gels *in situ*. Indeed, photo-crosslinked hydrogels are attractive for the design of bioadhesives that can be applied in minimally invasive surgery (e.g. for cell delivery[8]). As there was no significant difference found between the adhesion profiles of the gels to hydroxyl-functionalised slides compared with methacrylate-functionalised slides, bonding was evaluated directly against glass slides. Figure 5 and Figure 6 present the tensile bonding of the different gels to epicardium and gingiva, respectively. Failure for PAA-BA and PAA-Tyr, to both of these tissues, was cohesive (see Figure 5D and Figure 6D, respectively). Following testing, both gels presented clear surface coverage of the tissue surface,

indicating that bonding had occurred and failure occurred within the weak bulk of these gels. Similarly to results obtained on model substrates, PAA-BA and PAA-Tyr gels showed elastic deformation profiles (Figure 5B and Figure 6B). In addition, no significant difference in the adhesion strength was observed between PAA-BA and PAA-Tyr gels, to both the epicardium and gingiva.

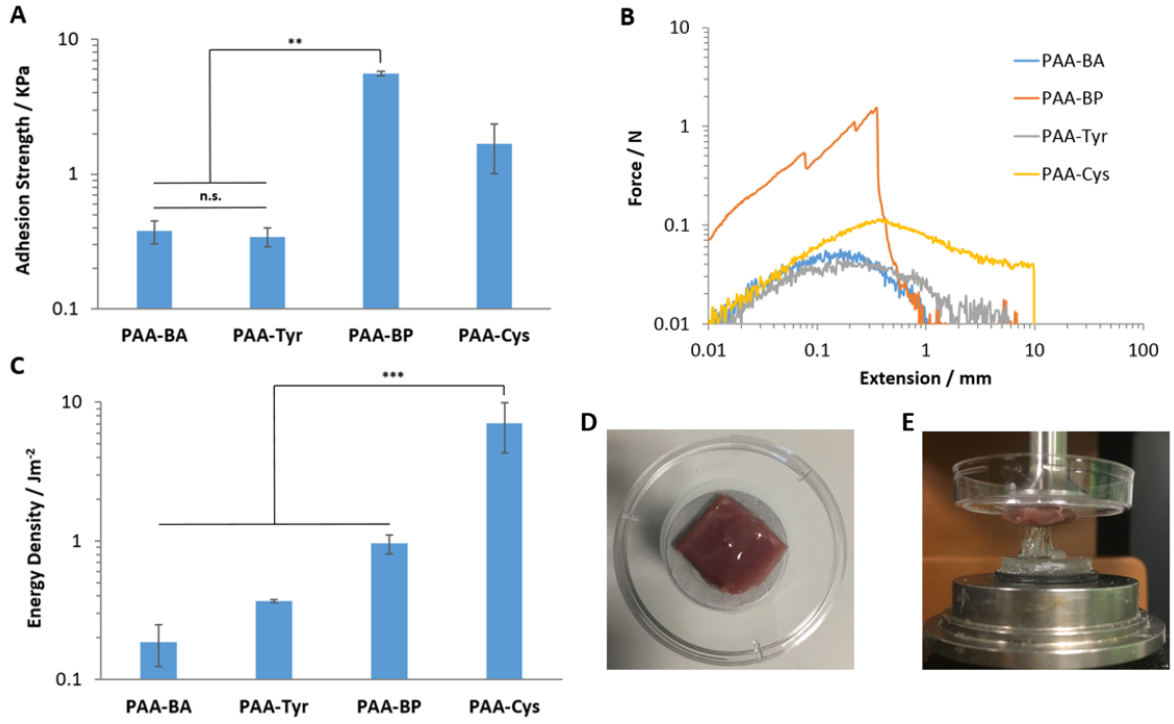

Figure 5. Tensile bond tests for adhesion of PAA-based hydrogels to porcine epicardium. (A) Adhesion strength of gels (maximum tensile force (N)/contact area (m^2)). (B) Force-extension for gels at a constant extension speed of 2.5 mm/min. (C) Energy density for gels (detachment work (J)/contact area (m^2)). (D) Image showing partial deposition of PAA-BA gel on epicardium surface following cohesive failure of the gel during testing. The gel can be seen to maintain near-complete wetting of the tissue surface. (E) Significant deformation observed for PAA-Cys gel during testing, with the formation of long fibres between the tissue and glass surface. Error bars show standard errors for repeats across samples (sample size $n \geq 3$). **, $p \leq 0.01$. ***, $p \leq 0.001$. n.s., non-significant.

Photo-radical initiated PAA-BP and PAA-Cys gels displayed stronger adhesion, although failure was adhesive in both cases (See Figure 5 and Figure 6). For PAA-Cys gels, failure occurred at the tissue interface for both epicardial and gingival samples. Similarly to what was observed on the model substrates, this gel displayed high elasticity and toughness, as a result of the combination of covalent and physical crosslinks, with failure only occurring at relatively large extensions (Figure 5B/E and Figure 6B). This is highlighted by the large energy densities calculated for adhesion to the epicardium and gingiva (energy densities of 7.1 Jm^{-2} and 12.8 Jm^{-2}, respectively; Figure 5C and Figure 6C). As these gels extended so significantly, with long fibres forming between the upper and lower substrates, the

tests were ended early, prior to complete failure of the sample. Consequently, there is a sudden drop in force at extensions of 10 mm when testing was ended. In terms of energy density, PAA-Cys gels displayed significantly greater adhesion to soft tissues than all other gels tested. In comparison to the data from the model substrates, this increase in energy density for PAA-Cys gels is thought to arise from increased reactivity with biomacromolecules at the tissue surface (e.g. via available cysteines) and partial interpenetration of the interfaces.

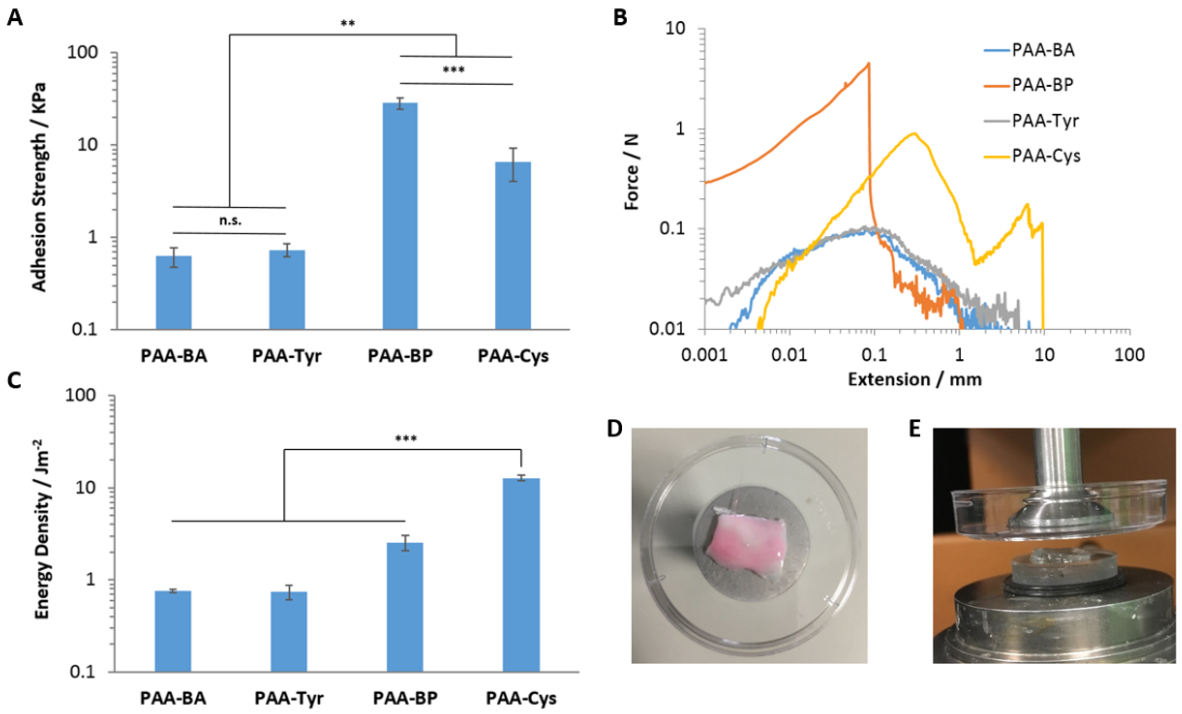

Figure 6. Tensile bond tests for adhesion of PAA-based hydrogels to porcine keratinized gingiva. (A) Adhesion strength of gels (maximum tensile force (N)/contact area (m^2)). (B) Force-extension for gels at a constant extension speed of 2.5 mm/min. (C) Energy density for gels (detachment work (J)/contact area (m^2)). (D) Image showing partial deposition of PAA-Tyr gel on gingiva surface following cohesive failure of the gel during testing. The gel can be seen to maintain near-complete wetting of the tissue surface. (E) Complete deposition of PAA-BP gel on glass surface following adhesive failure of gel at tissue interface. Error bars show standard errors for repeats across samples (sample size $n \geq 3$). **, $p \leq 0.01$. ***, $p \leq 0.001$. n.s., non-significant.

In contrast, PAA-BP gels adhesively failed at the glass interface for testing on epicardium tissue, and adhesively failed at the tissue interface in the case of the gingiva (Figure 6E). Similarly to the tests on model substrates, PAA-BP gels failed in a brittle manner with minimal extension of the gels occurring before failure at the tissue or glass interface (Figure 5B and Figure 6B). Accordingly, high adhesion strengths were measured (28.7 KPa for the gingiva; Figure 6A), and in comparison to PAA-Cys gels, slightly lower energy densities were recorded (2.6 Jm^{-2} for the gingiva; Figure 6C). Overall, tensile

bonding assays indicate excellent tissue bonding for PAA-BP, presumably due to the combined stiffness and chemical bonding of this gel with the tissue interface.

In terms of overall gel mechanics and tissue adhesion, one important contributing factor that should be highlighted is the functionalisation level for PAA (see

Table **1**). Unfortunately, matching degrees of functionalisation was not possible for the different chemistries selected. Differences in reactivities, but also in the solubility of the resulting polymers prevented us from achieving near 20% functionalisation in all cases. However, we aimed to promote the formation of stiffer and more strongly bonded hydrogels and therefore decided to use polymers with different degrees of substitution, despite the issue that this change brings about, in terms of comparing crosslinking and bonding. In the case of PAA-Cys and PAA-BP gels, functionalisation levels are sufficiently close (4.5 ± 0.1 and 4.4 ± 0.4%, respectively) that direct comparisons can be made between these two systems. For the other two gels, even though there are large differences in functionalisation levels, interesting comparisons can still be made and associated characteristics of the gelation systems can be inferred. As an example, despite the significantly higher functionalisation levels for PAA-BA (17.8 ± 0.3%), these gels still displayed comparatively weak mechanics and adhesion, as a result of the physical nature of their crosslinks. In addition, despite the low functionalisation levels of PAA-Tyr gels (1.8 ± 0.2%), in comparison to PAA-BA they still displayed excellent shear mechanics and soft tissue adhesion at a comparable level, reflecting the formation of stronger covalent crosslinks. However, in comparison to PAA-Cys and PAA-BP gels, the reduction in mechanics of PAA-Tyr is perhaps a result of the reduced functionalisation level achieved, but also as a result of the less efficient reaction between tyramine moieties.

Tissue adhesion was further characterised via lap shear experiments. Testing could only be carried out on gels that displayed sufficient mechanical strength, due to the vertical loading of samples in the testing apparatus. As such, testing was only carried out on PAA-BP and PAA-Cys. Similarly to results from tensile bond tests, PAA-BP and PAA-Cys gels displayed distinct modes of failure from one another, with PAA-BP gels displaying a more brittle mode of failure (Figure 7C) and PAA-Cys gels a more elastic one (Figure 7D).

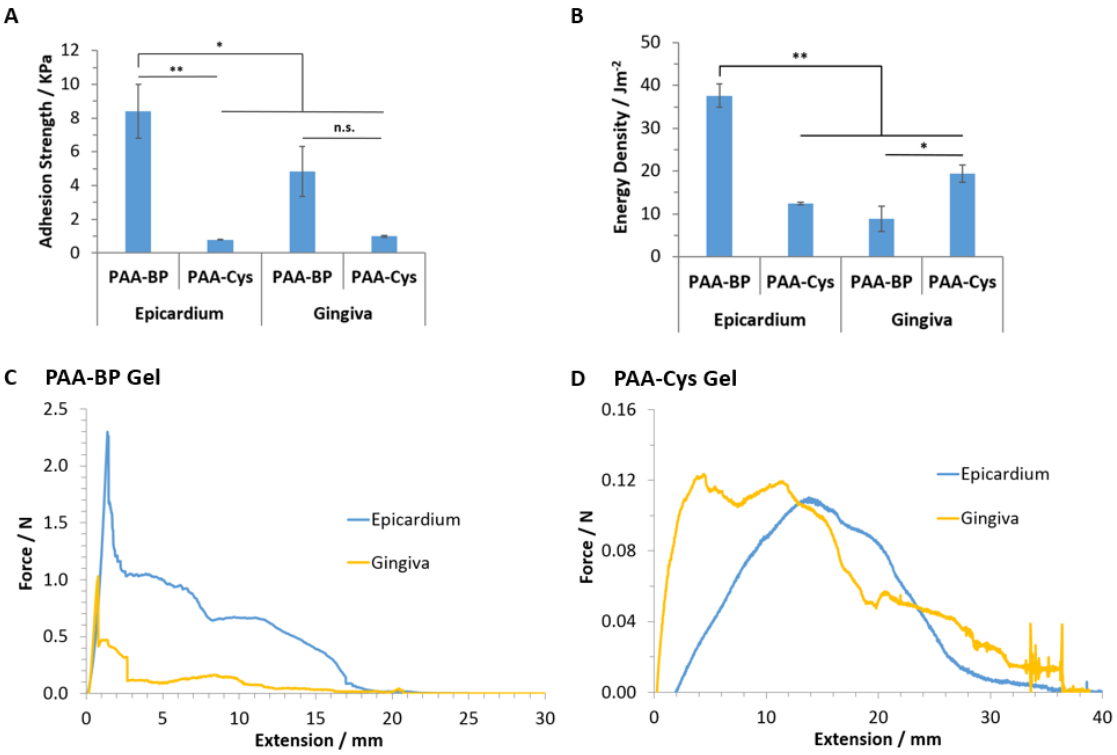

Figure 7. Lap shear tests for adhesion of PAA-BP and PAA-Cys hydrogels to porcine epicardium and keratinized gingiva at a constant extension speed of 10 mm/min. (A) Adhesion strength of gels (maximum tensile force (N)/contact area (m^2)). (B) Energy density for gels (detachment work (J)/contact area (m^2)). (C) Force-extension curves for PAA-BP gels. (D) Force-extension curves for PAA-Cys gels. Error bars show standard errors for repeats across samples (sample size $n \geq 3$). *, $p \leq 0.05$. **, $p \leq 0.01$. n.s., non-significant.

Failure of PAA-BP gels for tests on the epicardium, was adhesive at the glass interface, in line with strong adhesion previously reported for thiol-ene hydrogels to epicardium.[8] For tests on the gingiva, failure was adhesive again, occurring at both the glass or tissue interface across different repeats. These modes of failure are similar to those observed in the tensile bond tests and they suggest that PAA-BP gels are adhering to the epicardium with greater strength than to the gingiva. This is proposed to arise from differences in the surface chemistry of these tissues, notably a greater density of cysteines at the surface of epicardium, promoting enhanced bonding. In comparison to other tissue adhesives presented in the literature the PAA-BP hydrogels display comparatively high adhesion. A recent report by You *et al*. presented poly(2-alkyl-2-oxazoline) (POx)-based thiol-ene crosslinked hydrogels for epicardial placement and delivery of mesenchymal stromal cells (MSCs).[8] Lap shear adhesion characterisation of these gels to the epicardium was performed under identical conditions to the methodology used in the present report, and displayed significantly reduced adhesion strengths of all POx formulations used (< 3 KPa), in comparison to our PAA-BP gels (8.39 KPa; Figure 7A).

Moreover, tensile testing of commercial fibrin sealant to human soft tissue was reported to display an adhesive strength of 811 mN/cm^2.[81] For comparison, in our system, tensile adhesive strengths for PAA-BP were 560 and 2480 mN/cm^2, for the epicardium and gingiva respectively (values extracted and converted from Figure 5A and Figure 6A).

In addition to the impact of covalent bonding on the adhesion behaviour of the different systems studied, weaker hydrogen bonding, hydrophobic interactions and coulombic forces may also play a role in modulating tissue-specific responses. Indeed, it was previously reported that PAA brushes adhere more strongly to the epicardium compared to the gingiva.[67] This was found to be mediated by hydrogen bonding and hydrophobic forces primarily, based on comparison with model monolayers. Due to the relatively low functionalisation levels of our polymers studied (< 20% in all cases), such non-specific adhesion of PAA to tissues may impact on the overall adhesion behaviour observed. Colloidal probe AFM experiments also highlighted the strong influence of the cell glycocalyx (a proteoglycan brush-like layer that coats the cell membrane)[82] on such non-specific adhesion[67]. To the best of our knowledge, the epicardial glycocalyx has yet to be characterised. Accordingly, this study identifies a need for a more detailed characterisation of the surface chemistry of tissues to which biomaterials bonding is required.

For PAA-Cys gels, failure was adhesive and occurred at the tissue interface for tests on both the epicardium and gingiva. During testing of these gels, long fibres formed, bridging the gap between the upper and lower substrates and resulting in long extensions prior to complete failure (Figure 7D). Similarly to results from the tensile bond tests, the adhesion strength of PAA-Cys gels to each tissue type was significantly lower than that of PAA-BP gels (adhesions strengths < 0.99 KPa for PAA-Cys, compared with > 4.85 KPa for PAA-BP; Figure 7A). This difference was reduced in the case of energy density, and even inverted in the case of the gingiva (Figure 7B), potentially as a result of the increased viscoelasticity of PAA-Cys.

Finally, it should be pointed out that the mechanical properties of the tissue samples used will also likely contribute to the overall adhesion profiles measured. As the epicardium and gingiva have significantly different mechanical properties (Young's moduli of 20.7 and 1020 kPa, respectively, were quantified via nanoindentation[67]) this is expected to have some influence on the adhesion profiles observed for our gels. Evidence for the greater compliance of the epicardium, and the effect that this has on the results obtained, can be found when analysing force-extension profiles. Extension lengths at which the maximum force values are recorded are much greater for the epicardium compared with the gingiva (Figure 5B, Figure 6B and Figure 7C/D), indicating the influence of tissue deformation on the data obtained.

4. Conclusion

Our results indicate that hydrogel/soft tissue adhesion is regulated by a range of factors, including weak non-specific adhesion forces (the type of coupling that can occur between biomaterials and tissues), hydrogel and tissue mechanics, as well as potential interpenetration. In the context of the PAA hydrogels studied, covalent coupling mediated by thiol-ene chemistry, as in PAA-BP hydrogels, produces relatively high moduli and elasticity, whilst ensuring relatively strong coupling to tissues. Our study also highlights that thiol-thiol photo-mediated coupling is an attractive strategy to form disulfide networks that display increased viscoelasticity, compared to thiol-ene networks, potentially providing a path for energy dissipation and contributing to high extensibility and energy density. Hence, optimisation of the mechanical properties of these structures may results in particularly efficient bioadhesive hydrogels. Our results also indicate the importance of tissue biochemistry and the occurrence of reactive sites for coupling. The glycosylation and biochemistry of the glycocalyx present in the tissue of interest may significantly impact on adhesion and could potentially dominate adhesion properties. Hence, the integration of physical crosslinking to such interfaces, such as those mediated by boronic acids, could provide complementary physical crosslinks to enhance the strength of adhesion and ensure compatibility in more challenging environments. The design of such dual coupling systems remains limited, but could benefit from the flexibility of thiol-ene-mediated coupling.

Acknowledgement

Funding from the Engineering and Physical Sciences Research Council (grant EP/M507532/1) is gratefully acknowledged.

Supporting Information

Additional information available from XXXX.

References

1. Lee, Y. J. *et al.* Enhanced biocompatibility and wound healing properties of biodegradable polymer-modified allyl 2-cyanoacrylate tissue adhesive. *Mater. Sci. Eng. C* **51,** 43–50 (2015).

2. Petrie, E. M. Cyanoacrylate Adhesives in Surgical Applications. *Rev. Adhes. Adhes.* **2,** 253–310 (2014).

3. Ryssel, H., Gazyakan, E., Germann, G. & Öhlbauer, M. The use of MatriDerm® in early excision and simultaneous autologous skin grafting in burns-A pilot study. *Burns* **34,** 93–97 (2008).

4. Annabi, N. *et al.* Engineering a highly elastic human protein–based sealant for surgical applications. *Sci. Transl. Med.* **9,** eaai7466 (2017).

5. Li, J. *et al.* Tough adhesives for diverse wet surfaces. *Science (80-.).* **357,** 378–381 (2017).

6. Hoang Thi, T. T., Lee, Y., Ryu, S. B., Sung, H. & Park, K. D. Oxidized cyclodextrin-functionalized injectable gelatin hydrogels as a new platform for tissue-adhesive hydrophobic drug delivery. *RSC Adv.* **7,** 34053–34062 (2017).

7. Venugopal, J. R. *et al.* Biomaterial strategies for alleviation of myocardial infarction. *J. R. Soc. Interface* **9,** 1–19 (2012).

8. You, Y. *et al.* Engineered cell-degradable poly(2-alkyl-2-oxazoline) hydrogel for epicardial placement of mesenchymal stem cells for myocardial repair. *Biomaterials* 120356 (2020). doi:10.1016/j.biomaterials.2020.120356

9. Bhagat, V. & Becker, M. L. Degradable Adhesives for Surgery and Tissue Engineering. *Biomacromolecules* **18,** 3009–3039 (2017).

10. Samprasit, W. *et al.* Mucoadhesive electrospun chitosan-based nanofibre mats for dental caries prevention. *Carbohydr. Polym.* **117,** 933–940 (2015).

11. Tsibouklis, J., Middleton, A. M., Patel, N. & Pratten, J. Toward mucoadhesive hydrogel formulations for the management of xerostomia: The physicochemical, Biological, and Pharmacological Considerations. *J. Biomed. Mater. Res. - Part A* **101,** 3327–3338 (2013).

12. Marschütz, M. K. & Bernkop-Schnürch, A. Thiolated polymers: Self-crosslinking properties of thiolated 450 kDa poly(acrylic acid) and their influence on mucoadhesion. *Eur. J. Pharm. Sci.* **15,** 387–394 (2002).

13. Elliott, J. E., Macdonald, M., Nie, J. & Bowman, C. N. Structure and swelling of poly(acrylic acid) hydrogels: effect of pH, ionic strength, and dilution on the crosslinked polymer structure. *Polymer (Guildf).* **45,** 1503–1510 (2004).

14. Huang, Y., Yu, H. & Xiao, C. pH-sensitive cationic guar gum/poly (acrylic acid) polyelectrolyte hydrogels: Swelling and in vitro drug release. *Carbohydr. Polym.* **69,** 774–783 (2007).

15. Yin, M.-J. *et al.* Rapid 3D Patterning of Poly(acrylic acid) Ionic Hydrogel for Miniature pH Sensors. *Adv. Mater.* **28,** 1394–1399 (2016).

16. Dubolazov, A. V, Nurkeeva, Z. S., Mun, G. a & Khutoryanskiy, V. V. Design of mucoadhesive polymeric films based on blends of poly(acrylic acid) and (hydroxypropyl)cellulose. *Biomacromolecules* **7,** 1637–43 (2006).

17. Bromberg, L., Temchenko, M., Alakhov, V. & Hatton, T. A. Bioadhesive properties and

rheology of polyether-modified poly(acrylic acid) hydrogels. *Int. J. Pharm.* **282,** 45–60 (2004).

18. Nho, Y., Park, J. & Lim, Y. Preparation of Poly(acrylic acid) Hydrogel by Radiation Crosslinking and Its Application for Mucoadhesives. *Polymers (Basel).* **6,** 890–898 (2014).

19. De Giglio, E., Cometa, S., Cioffi, N., Torsi, L. & Sabbatini, L. Analytical investigations of poly(acrylic acid) coatings electrodeposited on titanium-based implants: A versatile approach to biocompatibility enhancement. *Anal. Bioanal. Chem.* **389,** 2055–2063 (2007).

20. Lee, W., Lee, T. G. & Koh, W. G. Grafting of Poly(acrylic acid) on the Poly(ethylene glycol) Hydrogel Using Surface-initiated Photopolymerization for Covalent Immobilization of Collagen. *J. Ind. Eng. Chem.* **13,** 1195–1200 (2007).

21. Zhao, X., Huebsch, N., Mooney, D. J. & Suo, Z. Stress-relaxation behavior in gels with ionic and covalent crosslinks. in *Journal of Applied Physics* **107,** (2010).

22. Wang, C., Yan, Q., Liu, H. B., Zhou, X. H. & Xiao, S. J. Different EDC/NHS activation mechanisms between PAA and PMAA brushes and the following amidation reactions. *Langmuir* **27,** 12058–12068 (2011).

23. Levy, T., Déjugnat, C. & Sukhorukov, G. B. Polymer Microcapsules with Carbohydrate-Sensitive Properties. *Adv. Funct. Mater.* **18,** 1586–1594 (2008).

24. Luo, Y., Ran, Q., Wu, S. & Shen, J. Synthesis and characterization of a poly(acrylic acid)-graft-methoxy poly(ethylene oxide) comblike copolymer. *J. Appl. Polym. Sci.* **109,** 3286–3291 (2008).

25. O'Boyle, N. M. *et al.* Synthesis and evaluation of antiproliferative microtubule-destabilising combretastatin A-4 piperazine conjugates. *Org. Biomol. Chem.* **17,** 6184–6200 (2019).

26. Colak, B., Di Cio, S. & Gautrot, J. E. Biofunctionalized Patterned Polymer Brushes via Thiol-Ene Coupling for the Control of Cell Adhesion and the Formation of Cell Arrays. *Biomacromolecules* **19,** 1445–1455 (2018).

27. Colak, B., Da Silva, J. C. S., Soares, T. A. & Gautrot, J. E. Impact of the Molecular Environment on Thiol-Ene Coupling for Biofunctionalization and Conjugation. *Bioconjug. Chem.* **27,** 2111–2123 (2016).

28. Ettehadi Gargari, J., Sid Kalal, H., Niknafs, D. & Khanchi, A. Synthesis of silica/PAA NPs via combining RAFT polymerization and thiol-ene click reaction and postpolymerization modifications with arsenazo (III). *Polym. Adv. Technol.* **29,** 2806–2815 (2018).

29. Chen, J. J., Struk, K. N. & Brennan, A. B. Surface modification of silicate glass using 3-(mercaptopropyl) trimethoxysilane for thiol-ene polymerization. *Langmuir* **27,** 13754–13761 (2011).

30. Loebel, C., D'Este, M., Alini, M., Zenobi-Wong, M. & Eglin, D. Precise tailoring of tyramine-based hyaluronan hydrogel properties using DMTMM conjugation. *Carbohydr. Polym.* **115,** 325–333 (2015).

31. Loebel, C., Broguiere, N., Alini, M., Zenobi-Wong, M. & Eglin, D. Microfabrication of Photo-Cross-Linked Hyaluronan Hydrogels by Single- and Two-Photon Tyramine Oxidation. *Biomacromolecules* **16,** 2624–2630 (2015).

32. Shu, X. Z., Liu, Y., Palumbo, F. & Prestwich, G. D. Disulfide-crosslinked hyaluronan-gelatin

hydrogel films: A covalent mimic of the extracellular matrix for in vitro cell growth. *Biomaterials* **24,** 3825–3834 (2003).

33. Shu, X. Z., Liu, Y., Luo, Y., Roberts, M. C. & Prestwich, G. D. Disulfide cross-linked hyaluronan hydrogels. *Biomacromolecules* **3,** 1304–1311 (2002).

34. Sun, Y. & Huang, Y. Disulfide-crosslinked albumin hydrogels. *J. Mater. Chem. B* **4,** 2768–2775 (2016).

35. Lee, K. Y. *et al.* Controlling mechanical and swelling properties of alginate hydrogels independently by cross-linker type and cross-linking density. *Macromolecules* **33,** 4291–4294 (2000).

36. Sato, T., Aoyagi, T., Ebara, M. & Auzély-Velty, R. Catechol-modified hyaluronic acid: in situ-forming hydrogels by auto-oxidation of catechol or photo-oxidation using visible light. *Polym. Bull.* (2017). doi:10.1007/s00289-017-1937-y

37. Gramlich, W. M., Kim, I. L. & Burdick, J. A. Synthesis and orthogonal photopatterning of hyaluronic acid hydrogels with thiol-norbornene chemistry. *Biomaterials* **34,** 9803–9811 (2013).

38. Shih, H. & Lin, C. C. Cross-linking and degradation of step-growth hydrogels formed by thiol-ene photoclick chemistry. *Biomacromolecules* **13,** 2003–2012 (2012).

39. Fairbanks, B. D., Schwartz, M. P., Bowman, C. N. & Anseth, K. S. Photoinitiated polymerization of PEG-diacrylate with lithium phenyl-2,4,6-trimethylbenzoylphosphinate: polymerization rate and cytocompatibility. *Biomaterials* **30,** 6702–6707 (2009).

40. Han, S. & Chien-Chi, L. Visible-Light-Mediated Thiol-Ene Hydrogelation Using Eosin-Y as the Only Photoinitiator. *Macromol. Rapid Commun.* **34,** 269–273 (2013).

41. Noshadi, I. *et al.* In vitro and in vivo analysis of visible light crosslinkable gelatin methacryloyl (GelMA) hydrogels. *Biomater. Sci.* **5,** 2093–2105 (2017).

42. Shih, H. & Lin, C. C. Visible-light-mediated thiol-ene hydrogelation using eosin-Y as the only photoinitiator. *Macromol. Rapid Commun.* **34,** 269–273 (2013).

43. Hao, Y., Shih, H., Muňoz, Z., Kemp, A. & Lin, C. C. Visible light cured thiol-vinyl hydrogels with tunable degradation for 3D cell culture. *Acta Biomater.* **10,** 104–114 (2014).

44. Tan, K. Y., Ramstedt, M., Colak, B., Huck, W. T. S. & Gautrot, J. E. Study of thiol–ene chemistry on polymer brushes and application to surface patterning and protein adsorption. *Polym. Chem.* **7,** 979–990 (2016).

45. Farrugia, B. L., Kempe, K., Schubert, U. S., Hoogenboom, R. & Dargaville, T. R. Poly(2-oxazoline) hydrogels for controlled fibroblast attachment. *Biomacromolecules* **14,** 2724–2732 (2013).

46. Khetan, S., Katz, J. S. & Burdick, J. A. Sequential crosslinking to control cellular spreading in 3-dimensional hydrogels. *Soft Matter* **5,** 1601–1606 (2009).

47. Colak, B., Wu, L., Cozens, E. J. & Gautrot, J. E. Modulation of Thiol–Ene Coupling by the Molecular Environment of Polymer Backbones for Hydrogel Formation and Cell Encapsulation. *ACS Appl. Bio Mater.* (2020). doi:10.1021/acsabm.0c00908

48. Kade, M. J., Burke, D. J. & Hawker, C. J. The power of thiol-ene chemistry. *J. Polym. Sci. Part A*

Polym. Chem. **48,** 743–750 (2010).

49. Su, J. Thiol-Mediated Chemoselective Strategies for In Situ Formation of Hydrogels. *Gels* **4,** 72 (2018).

50. Yan, X., Yang, X., Tong, X. & Huang, Y. A method to accelerate the gelation of disulfide-crosslinked hydrogels. *Chinese J. Polym. Sci. (English Ed.* **33,** 118–127 (2015).

51. Goessl, A., Tirelli, N. & Hubbell, J. A. A hydrogel system for stimulus-responsive, oxygen-sensitive in situ gelation. *J. Biomater. Sci. Polym. Ed.* **15,** 895–904 (2004).

52. Guan, Y. & Zhang, Y. Boronic acid-containing hydrogels: synthesis and their applications. *Chem. Soc. Rev.* **42,** 8106 (2013).

53. Wu, X. *et al.* Selective sensing of saccharides using simple boronic acids and their aggregates. *Chem. Soc. Rev.* **42,** 8032–48 (2013).

54. Xu, Z., Deng, P., Tang, S. & Li, J. Fluorescent boronic acid terminated polymer grafted silica particles synthesized via click chemistry for affinity separation of saccharides. *Mater. Sci. Eng. C* **40,** 228–234 (2014).

55. Heleg-Shabtai, V., Aizen, R., Orbach, R., Aleman-Garcia, M. A. & Willner, I. Gossypol-cross-linked boronic acid-modified Hydrogels: A functional matrix for the controlled release of an anticancer drug. *Langmuir* **31,** 2237–2242 (2015).

56. Deng, C. C., Brooks, W. L. A., Abboud, K. A. & Sumerlin, B. S. Boronic acid-based hydrogels undergo self-healing at neutral and acidic pH. *ACS Macro Lett.* **4,** 220–224 (2015).

57. Sun, J.-Y. *et al.* Highly stretchable and tough hydrogels. *Nature* **489,** 133–136 (2012).

58. Henderson, K. J., Zhou, T. C., Otim, K. J. & Shull, K. R. Ionically cross-linked triblock copolymer hydrogels with high strength. *Macromolecules* **43,** 6193–6201 (2010).

59. Webber, R. E., Creton, C., Brown, H. R. & Gong, J. P. Large strain hysteresis and mullins effect of tough double-network hydrogels. *Macromolecules* **40,** 2919–2927 (2007).

60. Yu, Q. M., Tanaka, Y., Furukawa, H., Kurokawa, T. & Gong, J. P. Direct observation of damage zone around crack tips in double-network gels. *Macromolecules* **42,** 3852–3855 (2009).

61. Bjork, J. W., Johnson, S. L. & Tranquillo, R. T. Ruthenium-catalyzed photo cross-linking of fibrin-based engineered tissue. *Biomaterials* **32,** 2479–2488 (2011).

62. Lim, K. S., Alves, M. H., Poole-Warren, L. A. & Martens, P. J. Covalent incorporation of non-chemically modified gelatin into degradable PVA-tyramine hydrogels. *Biomaterials* **34,** 7097–7105 (2013).

63. Araña, M. *et al.* Epicardial delivery of collagen patches with adipose-derived stem cells in rat and minipig models of chronic myocardial infarction. *Biomaterials* **35,** 143–151 (2014).

64. Tano, N. *et al.* Epicardial placement of mesenchymal stromal cell-sheets for the treatment of ischemic cardiomyopathy; In vivo proof-of-concept study. *Mol. Ther.* **22,** 1864–1871 (2014).

65. Megone, W., Roohpour, N. & Gautrot, J. E. Impact of surface adhesion and sample heterogeneity on the multiscale mechanical characterisation of soft biomaterials. *Sci. Rep.* **8,** 1–10 (2018).

66. Wu, L., Di Cio, S., Azevedo, H. S. & Gautrot, J. E. Photoconfigurable, Cell-Remodelable Disulfide Cross-linked Hyaluronic Acid Hydrogels. *Biomacromolecules* (2020). doi:10.1021/acs.biomac.0c00603

67. Cozens, E. J., Kong, D., Roohpour, N. & Gautrot, J. E. The physico-chemistry of adhesions of protein resistant and weak polyelectrolyte brushes to cells and tissues. *Soft Matter* **16,** 505–522 (2020).

68. D'Este, M., Eglin, D. & Alini, M. A systematic analysis of DMTMM vs EDC/NHS for ligation of amines to Hyaluronan in water. *Carbohydr. Polym.* **108,** 239–246 (2014).

69. Thompson, K. & Michielsen, S. Novel synthesis of N-substituted polyacrylamides: Derivatization of poly(acrylic acid) with amines using a triazine-based condensing reagent. *J. Polym. Sci. Part A Polym. Chem.* **44,** 126–136 (2006).

70. Pelet, J. M. & Putnam, D. An in-depth analysis of polymer-analogous conjugation using DMTMM. *Bioconjug. Chem.* **22,** 329–337 (2011).

71. Kunishima, M. *et al.* 4-(4,6-dimethoxy-1,3,5-triazin-2-yl)-4-methyl-morpholinium chloride: an efficient condensing agent leading to the formation of amides and esters. *Tetrahedron* **55,** 13159–13170 (1999).

72. Raw, S. A. An improved process for the synthesis of DMTMM-based coupling reagents. *Tetrahedron Lett.* **50,** 946–948 (2009).

73. Davis, K. a. & Matyjaszewski, K. Atom transfer radical polymerization of tert-butyl acrylate and preparation of block copolymers. *Macromolecules* **33,** 4039–4047 (2000).

74. Lego, B., Skene, W. G. & Giasson, S. Swelling Study of Responsive Polyelectrolyte Brushes Grafted from Mica Substrates: Effect of pH, Salt, and Grafting Density. *Macromolecules* **43,** 4384–4393 (2010).

75. Grabowska, B. & Holtzer, M. Structural examination of the cross-linking reaction mechanism of polyacrylate binding agents. *Arch. Metall. Mater.* **54,** 427–437 (2009).

76. Faniran, J. A. & Shurvell, H. F. Infrared spectra of phenylboronic acid (normal and deuterated) and diphenyl phenylboronate. *Can. J. Chem.* **46,** 2089–2095 (1968).

77. Wang, Y. M. *et al.* Poly(acrylic acid) brushes pattern as a 3D functional biosensor surface for microchips. *Appl. Surf. Sci.* **266,** 313–318 (2013).

78. Tavakkoli Yaraki, M. *et al.* Synthesis and optical properties of cysteamine-capped ZnS quantum dots for aflatoxin quantification. *J. Alloys Compd.* **690,** 749–758 (2017).

79. Jay, J. I., Langheinrich, K., Hanson, M. C., Mahalingam, A. & Kiser, P. F. Unequal stoichiometry between crosslinking moieties affects the properties of transient networks formed by dynamic covalent crosslinks. *Soft Matter* **7,** 5826–5835 (2011).

80. He, L., Fullenkamp, D. E., Rivera, J. G. & Messersmith, P. B. PH responsive self-healing hydrogels formed by boronate-catechol complexation. *Chem. Commun.* **47,** 7497–7499 (2011).

81. Kjaergard, H. K., Velada, J. L., Pedersen, J. H., Fleron, H. & Hollingsbee, D. A. Comparative kinetics of polymerisation of three fibrin sealants and influence on timing of tissue adhesion. *Thromb. Res.* **98,** 221–228 (2000).

82. Weinbaum, S., Tarbell, J. M. & Damiano, E. R. The Structure and Function of the Endothelial Glycocalyx Layer. *Annu. Rev. Biomed. Eng.* **9,** 121–167 (2007).